Journal of Applied Polymer Science

WILEY

Applied Polymer SCIENCE

RESEARCH ARTICLE OPEN ACCESS

Characterization of Lightweight Polymeric Honeycomb Structures for Use as Backsides in Glass-Free PV Modules

Nikolina Pervan[1,2] | Umang Desai[3] | Gabriele C. Eder[4] | Jonathan Govaerts[5] | Arne Derluyn[6] | Wouter Winant[6] | Antonin Faes[3] | Christophe Ballif[3] | Gernot Oreski[1,2]

[1]Polymer Competence Center Leoben GmbH (PCCL), Leoben, Austria | [2]Montanuniversität Leoben, Leoben, Austria | [3]École Polytechnique Fédérale de Lausanne (EPFL), Lausanne, Switzerland | [4]Österreichisches Forschungsinstitut für Chemie und Technik (OFI), Vienna, Austria | [5]Interuniversity Microelectronics Centre (imec), Genk, Belgium | [6]EconCore N.V, Leuven, Belgium

Correspondence: Nikolina Pervan (nikolina.pervan@unileoben.ac.at; nikolina.pervan@pccl.at) | Gernot Oreski (gernot.oreski@unileoben.ac.at)

Received: 19 May 2025 | **Revised:** 14 August 2025 | **Accepted:** 18 August 2025

Funding: Solar Era Net Project "DELIGHT," co-fund by Austrian Research Promotion Agency (FFG, contract number FO999897443) and Swiss Federal Office of Energy (SFOE, contract number SI/502501-01).

Keywords: aging | backsheets | building applied photovoltaic modules | composites | glass-free | lightweight | material characterization | optical and photovoltaic applications | thermal properties | thermoplastics

ABSTRACT

In densely populated or mountainous countries where installation of large-scale solar plants is challenging, photovoltaic (PV) modules in building applications offer a solution by transforming passive surfaces into energy-generating systems. The need for flexible, lightweight, and "invisible" PV modules, with a life-time of over 20 years, comparable performance to the standard modules, and enabled recyclability resulted in various designs on the market. This research focuses on thermoplastic honeycomb sandwich composites (HSCs) with glass fiber-reinforced polymer skins as potential lightweight backsides for PV modules. Through material characterization and damp heat testing, their optical, mechanical, and thermal performance, compatibility with lamination processes, and ability to protect internal components from UV radiation and humidity were evaluated. Results show that proper glass fiber embedment improves mechanical properties and reduces water vapor transmission rates. Semitransparent skins could enable bifacial PV modules but require UV absorbers for long-term stability. HSCs exhibit glass-like thermomechanical behavior but low thermal conductivity, which could affect module temperature regulation. Damp heat exposure caused minor degradation in PP-based materials, while PET materials experienced polymer chain-scission and significant material embrittlement, which indicates the need for improved hydrolysis resistance.

1 | Introduction

The European Green Deal incentivizes increasing the share of renewable energy in the energy mix by at least 40% by 2030 [1]. With this goal, Europe is setting a path for becoming the first carbon-neutral continent by 2050. Although solar power is one of the highest energy-dense renewable sources, its energy density remains low compared to fossil fuels [2]. As a result, large areas must be covered with photovoltaic (PV) modules to generate sufficient energy and meet carbon neutrality [3]. Countries that are either densely populated or have mountainous terrains, such as the Netherlands, Switzerland, and Austria, face challenges in increasing their share of renewable energy produced by solar power due to limited available land for large-scale PV plants.

Building-integrated and building-attached PV (BIPV and BAPV) installations offer a solution by converting "passive" building areas into active renewable energy sources and CO_2

neutral areas [4]. However, PV module integration is not without obstacles; despite the numerous benefits it offers, it also presents challenges.

Current standard PV modules, which consist of a glass backsheet, encapsulant, solar cells with interconnections, glass frontsheet, junction box, and frame, are not a one-size-fits-all solution. Based on technical data sheets from various PV module producers, these modules can weigh up to 20 kg m^{-2}, and with racking systems potentially up to 40 kg m^{-2}. BIPV modules must comply with both PV and building standards/codes, as they have to fulfill a dual role as a building element and an electrotechnical energy generator, where IEC 63092 combines both aspects [4]. Mechanical stability and fire safety are of utmost importance for both BIPV and BAPV systems [5, 6], and standard 3.2 mm glass/glass PV modules typically pass certification with ease.

However, industrial and commercial buildings, as well as historical or heritage buildings may not be able to bear the structural load of these relatively heavy modules. In addition, the predominantly flat geometry, the lack of flexibility, and the "typical" dark, boxed, and rectangular appearance of standard PV modules often do not meet the aesthetic requirements of modern and historical architecture [7], where the aim is to integrate PV modules seamlessly with the building's design, often concealing them within the structure [4]. This can be achieved by hiding solar cells with colored encapsulant and frontsheet foils [8], by opting for thin film solar cell technology or c-Si cell technology for flexible designs [9].

Growing demand for innovative PV module designs specifically tailored for BIPV and BAPV applications is still on the rise. The need for flexible, lightweight, and "invisible" PV modules has opened doors for creativity in the PV industry [10], emphasizing the importance of ensuring that new designs still achieve a service life exceeding 20 years, maintain the performance of standard modules, prioritize recyclability and circularity while remaining cost-effective [5].

In an effort to reduce the weight of integrated/attached PV modules while maintaining or even enhancing mechanical stability, various "sandwich" composite solutions have been tested and integrated as backsides of PV modules [11–16]. Martins et al. investigated the use of honeycomb composite structures as backsides for PV modules. The lamination of these composite structures was done using EVA, ionomer, and thermoplastic polyolefin (TPO) encapsulants, which served as the adhesion layer between the Nomex or aluminum core and the glass fiber reinforced polymer (GFRP) skins. The honeycomb structures showed good mechanical stability even after undergoing thermal cycling and damp heat (DH) tests. PV modules incorporating these backsides exhibited favorable electrical performance, with a power loss of 2%–3% after undergoing artificial aging tests [12]. Kutter et al. introduced a rigid and torsion-resistant sandwich composite composed of polyurethane foam as the core and GFRP skins, aimed as a backside for lightweight PV modules. Their modules were subjected to artificial aging, and the degradation effect was observed following the DH exposure. This resulted in the embrittlement of the GFRP skin, allowing water ingress that led to corrosion of the interconnections. In contrast, thermal cycling and ultraviolet (UV) weathering had no observable impact on the backsheet [16]. Additionally, Alanis et al. conducted simulations to assess the thermal effects of integrating lightweight PV modules with sandwich composites as backside into the box body of refrigerated cargo trucks, confirming their findings through a mini-PV module experimental setup. Their research indicates that, in addition to providing good mechanical properties, sandwich composite structures can help insulate substrates (such as roofs and walls) to which PV modules are attached from the heat generated by the solar cells [17].

As previously mentioned, reducing weight and costs, along with introducing design flexibility, is a key driving factor in the development of glass-free PV modules. While enabling new designs through versatile backsheets, it is important not to neglect the functional role of the backsheet in PV modules. New designs must still protect the internal components from external factors such as gases, humidity, and UV radiation, while providing mechanical stability and electrical insulation of the active part of the PV module [18–20].

Even though sandwich structures with GFRP skins and aluminum or Nomex core materials fulfill the role of a structural backside [12], the high costs of Nomex and the potential for poor electrical insulation of the aluminum core have motivated the investigation of thermoplastic honeycomb sandwich composite (HSC) as a potential substitute for backside material in lightweight PV modules. In this study, commercially available polymeric HSC, already used in building and automotive industries, have been selected and evaluated for their suitability as backsides for PV modules. During material selection, it was ensured that the composites were free of fluorinated compounds, cost-effective, and potentially recyclable. Material characterization was conducted at the component level in accordance with PV standards, including Series IEC 62788 and IEC Technical Specification and the fire tests described in IEC 61730-2 [4], to assess the general, optical, mechanical, and thermal properties of the materials. The objective of this assessment was to determine whether the composites could be integrated into the standard lamination process for the PV module production, evaluate their effectiveness in protecting internal components from environmental influences, for example, UV, temperature, humidity, and analyze the material state after exposure.

Inadequate or improper testing may result in unsuitable materials entering the market and lead to PV failures, which may cause economic losses as well as adverse environmental and health impacts (release of F-reach gasses in case of PV module burning). Testing protocols are not infallible, as it is difficult to predict every environmental stressor and potential interaction that could influence material performance, aging, and degradation. While long-term outdoor testing can provide definitive information on material performance [21], it is time-consuming. Therefore, indoor artificial aging tests and material characterization [22] can sufficiently define material properties to either approve or disqualify specific materials for PV applications.

TABLE 1 | Composition and dimensional properties of HSC with polypropylene (PP) and recycled polyethylene terephthalate (rPET) cores; glass fiber reinforced (GFR) PP, GFR polyethylene terephthalate glycol (PETg), and biaxially oriented (BO)PET skins.

Sample (core_skin)	Core material	Skin material	Areal weight ($kg\,m^{-2}$)	Thickness sandwich (mm)	Thickness skin (mm)
PP80_PP1	PP	GFR PP	2.30	12.00	0.40
PP120_PP2	PP	GFR PP	2.97	11.80	0.47
PP120_PP3	PP	GFR PP	3.37	12.00	0.55
PET80_PET1	rPET	GFR PETg	2.51	10.30	0.48
PET80_PET2	rPET	BOPET	1.82	10.50	0.25

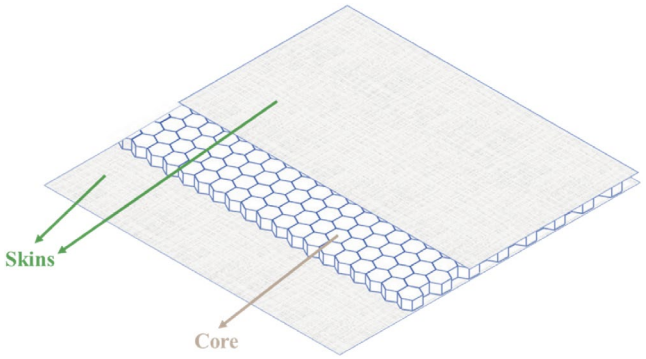

FIGURE 1 | Scheme of a honeycomb sandwich composite structure. [Color figure can be viewed at wileyonlinelibrary.com]

2 | Experimental Section

2.1 | Materials

Five different polymeric HSCs provided by EconCore N.V., Belgium, have been selected as potential PV backsides; details on their composition are given in Table 1, and the structure is shown in Figure 1. The materials were characterized both prior to and post accelerated aging exposure, with all tests conducted in three repetitions to minimize experimental errors.

2.2 | Accelerated Aging

2.2.1 | DH

Series of PV module laminates with PP and PET based HSC as backsides were prepared as described in [23] and exposed to DH conditions of 85°C and 85% humidity for 1000 h, following IEC 61215 MGT 13 [23, 24]. After accelerated aging, samples were taken from both the skin and the core of the HSC for thermal characterization and determination of material durability towards DH conditions.

2.2.2 | Water Condensation

To investigate water condensation within the hollow cell space of the core layer, HSC panels were cut into $10 \times 10\,cm^2$ samples. Aluminum adhesive tape was applied on the edges and rear side of the panels to mimic realistic conditions in a PV module, where the inner side of the backsheet is sealed with the encapsulant and frontsheet, and the edges are sealed with either a frame or an edge seal. The samples were dried at 40°C for 48 h to obtain the initial weight and then placed in a Weiss WLK 64-40 climate chamber. Continuous heating and cooling cycles from 85°C to 5°C and 85% humidity were maintained for 30 days. Samples were kept at 85°C for 18 h and at 5°C for 5 h. The weight of the samples was measured at the end of the cooling cycle. After 30 days, the samples were dried again at 40°C for 48 h and the weight was measured post-drying.

2.3 | Material Characterization

2.3.1 | Microscope Imaging

Light microscopic images of the skin material embedded in epoxy resin were taken with a Light Microscope MAT 7 from Carl Zeiss GmbH, in the bright field mode.

2.3.2 | UV–vis–NIR

Hemispherical transmittance of the independent skins was recorded over the wavelength range between 250 and 2500 nm with a Lambda 950 Ultra Violet-Visible–Near Infrared (UV–vis–NIR) Spectrophotometer (PerkinElmer Inc.).

2.3.3 | Differential Scanning Calorimetry (DSC)

DSC was performed using a DSC 6000 from PerkinElmer Inc. to measure thermograms of each polymeric component material, core and skin, separately. Approximately 10 mg of each material was placed in an aluminum pan with a perforated lid and subjected to a first heating run from −60°C to 300°C, followed by a cooling run from 300°C to −60°C and a second heating run from −60°C to 300°C. The heating rates were set to $10\,K\,min^{-1}$ and a nitrogen flow of $50\,mL\,min^{-1}$ was imposed.

2.3.4 | Heat Conductivity

The heat flow through the HSC samples was measured using a Guarder Heat Flow (GHF) Meter DTC-300 from TA Instruments (thermal conductivity tester). For this purpose,

the samples were cut into round specimens with a diameter of ∅50 mm. The sample was placed between an upper "hot" and a lower "cold" plate. The upper plate is heated to a temperature 15°C higher, and the lower plate is cooled to a temperature 15°C lower than the temperature at which material's heat conductivity is to be determined. Heat flows through the sample from the hot to the cold plate until thermal equilibrium is reached. The heat conductivity is calculated using Fourier's law:

$$\lambda = \frac{\dot{Q}\, d}{A \Delta T} \tag{1}$$

where Q is the heat flow throughout the specimen in W, d is the thickness in m, A is the area in m^2, and ΔT is the temperature difference across the sample in K [25].

2.3.5 | Coefficient of Thermal Expansion (CTE)

The CTE was measured using a Dantec Q400 TCT (Dantec Dynamics) Digital Image Correlation (DIC) system. The device consists of two cameras and a heating/cooling concealed chamber equipped with a thermal plate. Time series of images of the measured sample are taken during the thermal stages, which are then compared to the initial picture. During analysis, the evaluation software Istra 4D (Dantec Dynamics) calculates the relative displacement between the reference and each image of the acquired time series. Sample preparation is important as the software follows a speckle pattern that is applied on the surface of the rectangular sample of $3 \times 3\,cm^2$. The speckle pattern was applied on the skin of the HSC in two layers; the first white coating serves as a primer and substrate cover and is followed by a second layer that is a black coating which is creating the speckle pattern. Achieving good contrast and independent speckles is necessary to guarantee a measurable surface area. The CTE of the honeycomb composites was measured in the temperature range from −50°C to 120°C, with a heating rate of $2\,K\,min^{-1}$.

2.3.6 | Thermogravimetric Analysis (TGA)

TGA was done using a Thermogravimetric System TGA/DSC 1 of Mettler Toledo GmbH. The weight loss of approximately 10 mg of material was monitored while heating the sample in nitrogen atmosphere ($50\,mL\,min^{-1}$) from 35°C to 700°C, with a heating rate of $10°C\,min^{-1}$. The temperature at which the weight loss is equal to 5% with respect to the initial value ($=T_{5\%}$) is considered an indicator for the beginning of the material's decomposition process.

2.3.7 | Mechanical Properties

Zwick Universal Testing Machine (Z020) was used, with a load cell of 1 kN capacity, to perform 4-point bending tests at room temperature on the HSC samples to compare the mode of failure and the flexural rigidity. The tests were performed on the samples of 220 mm length and 25 mm width with a $20\,\mu m\,s^{-1}$ loading rate, 190 mm outer span length, and 90 mm inner span length, in the transversal direction to the core cells, as described in [26].

3 | Results and Discussion

Optimal qualification of the HSCs as a suitable "backsheet" option for PV modules can be achieved by comparing its properties to those of the most commonly used polymer composite backsheet Tedlar-PET-Tedlar (TPT) and the glass backsheet. Summary of all results is presented in Table 2.

3.1 | Physical Properties

The quality of embedment of the glass fibers (GFs) within the skin-sheets was investigated first, as the importance of proper impregnation of GFs within the polymer matrix and its influence on material properties, such as mechanical strength, water vapor, and gas permeation, has been emphasized multiple times in the literature [29, 34–36]. Common processing defects within GFRPs include voids in the form of entrapped air bubbles, insufficient wetting of the GFs with polymer, cracking of the polymer matrix in areas with fiber bundles, and delamination of the layer stack [36] Such defects might negatively impact the mechanical strength and increase the permeation of humidity, oxygen, or other gases in the skins of the HSCs under study. Thus, the water vapor transmission rate (WVTR) of all skin materials was measured and compared to standard PV backsheet materials [36] as it is known to be critical when selecting components for PV modules. Ingress of humidity into the module can lead to degradation of internal components including delamination, yellowing, and hazing of encapsulants, power loss in solar cells, corrosion of interconnection, and ultimately, PV module failure [37–40].

Microscopic images of the cross-sections of the GFR PP skins PP1–PP3 and the PET1 skin are shown in Figure 2. Differences in the GF distribution, for example, formation of fiber bundles, voids, and microcracks in the matrix of the skins are visible. The increase in thickness from PP1 to PP3 is due to the higher content of both GFs and the polymer matrix. With the increase in the amount of polymer in the composite, a decrease in WVTR is expected. The WVTR of these HSC skins was measured by Babin et al. [34]; the results confirm that lower WVTRs were observed for GFRP sheets with a thicker outer polymer layer covering the GFs (Sample PP3), see Figure 3. In contrast, higher WVTRs were measured for samples where the GFs were poorly covered with a thin polymer layer (Sample PP1). The type of polymer matrix also affects the WVTR of GFRP. This becomes evident when comparing the WVTRs of the skin sheets with the PET polymer matrix (Sample PET1, value WVTR) and that with the PP polymer matrix (Sample PP2, value WVTR), despite the samples having the same thickness and GF distribution (see Table 1 and Figure 4) [29]. In addition to increasing the thickness of the outer polymer layer and providing better coverage/embedment of the GFs, a gel coat can be applied to the outer GFRP skin layer to further decrease the water vapor permeability, enhance UV resistance, and, in special formulation, increase fire resistance [41–43].

The light transmittance of PV module backsides, for example, blocking of UV light is particularly important, as it can lead to degradation of internal components, thereby reducing the efficiency and lifetime performance of PV modules [18]. On the

TABLE 2 | Summary of the PP and PET HSC, TPT, and glass backsheet properties, including the effect which HSC could bring onto the PV module.

Property	Backsheet[a]	Glass	PP HSC	PET HSC	Effect of the HSC as a backsheet to the PV module
Thickness (mm)	0.2–0.4 [20]	3.2	11.8–12	10.3–10.5	Thicker PV module—need for new frame design.
Areal weight ($kg\,m^{-2}$)	~0.5[b] [27]	8 [28]	2.3–3.4	1.8–2.5	Significant reduction of weight compared to glass backsheet.
Mechanical strength	weak	strong	GFR skin dependent	Brittle	Replacement of the glass frontsheet as well as the removal of the aluminum frame feasible for PP based HSC.
WVTR ($g\,day^{-1}\,m^{-2}$)	< 1 [20]	$<10^{-6}$	2–8 [29]	0.7–1.2 [29]	WVTR are high and could lead to degradation of the inner components (corrosion, solar cell degradation, encapsulant degradation—delamination).
UV transmission (250–380 nm)	Cut off	90%	< 40%	Cut off at 310 nm	UV absorbers must be added in the polymer matrix to protect backsheet and inner components from photooxidation.
Degradation onset T ($T_{5\%}$—°C)	> 380[c]	—	> 430	> 400	Some backsheets have fire-retardant properties in comparison to the pure PP and PET, on the other hand they can generate toxic gas and toxic residues [30].
Melting temperature (°C)	195 [31]	—	145–175	> 230	PP HSC unsuitable for standard lamination process at 160°C, suitable for noncrosslinking encapsulants such as TPO.
CTE at 25°C (ppm)	> 30[d]	7[c]	6–12[d]	10–17[d]	Similar to the glass, should not result in delamination.
Heat conductivity ($W\,m^{-1}\,K^{-1}$)	0.15 [32]	1 [33]	~0.15	~0.15	Benefit: insulation towards the building Challenge: Potential slower cooling of the PV module—decrease in efficiency.
Accelerated aging	Weak impact	No impact	Material dependent	Material dependent	Chain scission in PET material led to material embrittlement—antihydrolysis additive for polymer matrix necessary.

[a]Standard laminated backsheet with PET core layer.
[b]Calculated from density for 0.34 mm thickness.
[c]Measured at PCCL.
[d]T dependent.

contrary, the transmittance of UV and visible light through the backsheets is beneficial for the yield of bifacial PV modules, as light can be absorbed by the rear side of the cells, converted into electricity, and increase power generation.

PP2, a dark black skin with unspecified additives (most likely carbon black), effectively blocks both visible and UV light. In contrast, PP1, PP3, PET1, and PET2 are semitransparent skins, with visible light transmittance ranging from 38% to 88% (see Figure 4), offering potential for bifacial PV modules. The disadvantage of these semitransparent skins, however, is that the transmitted UV radiation can cause photo-oxidative degradation of the HSC skins and the core. To block or minimize UV transmission, these materials would need to be adapted or supported with additional layers. This can be achieved through the addition of UV absorbers to the polymer

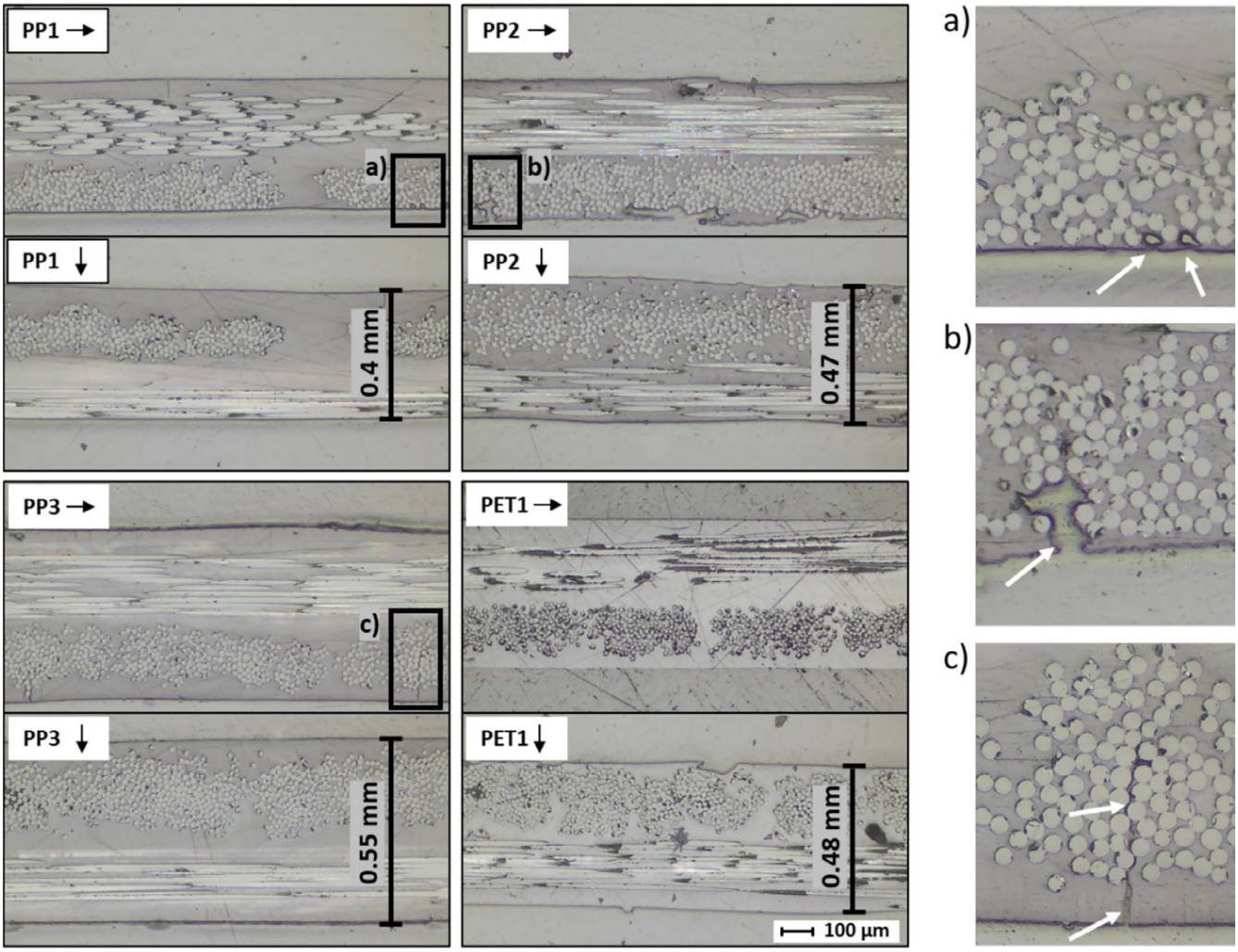

FIGURE 2 | Microscope images of the GFR honeycomb skin cross-sections and polymer matrix defects (a) small air bubble entrapment, (b) large air bubble entrapment, and (c) crack due to the fiber bundle. [Color figure can be viewed at wileyonlinelibrary.com]

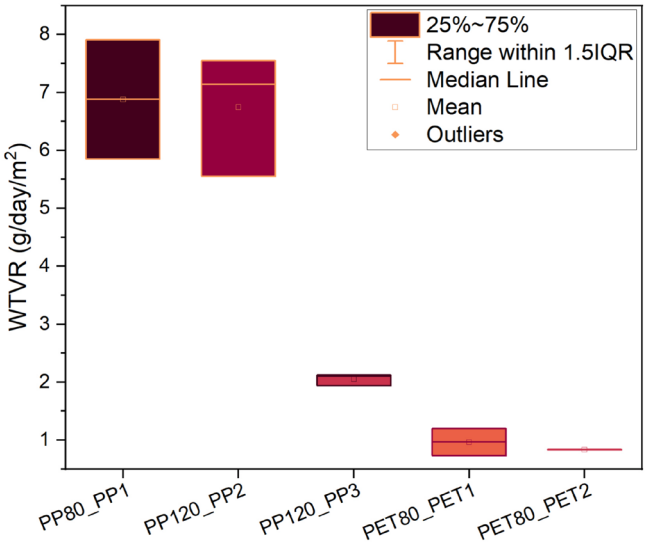

FIGURE 3 | WVTR of HSC skins (recalculated from [29] for the exact thickness of material, instead of WVTR values per 100 µm). [Color figure can be viewed at wileyonlinelibrary.com]

matrix or by applying an external UV-blocking coating to the outer skin layer in combination with a UV-blocking encapsulant on the cell backside.

3.2 | Thermal Properties

Thermal properties of polymer materials are of great significance when designing PV modules. First, during the lamination process of PV module production, which occurs at high temperatures (~150°C) and vacuum pressure (up to 1 bar), all components, besides encapsulating material, must remain dimensionally intact (minimal shrinkage, compression, deformation). Second, throughout the lifetime of a PV module, it will undergo thermal fluctuations (day—night and summer—winter).

The glass transition/softening (T_g) and melting (T_m) temperatures of the HSC components are of special interest to determine the optimal PV module lamination temperatures to avoid structural and dimensional changes of the backsheet material. The first heating thermograms (see Figure 5) show

the thermal behavior of the material before it undergoes the lamination process. The PP HSC components melt in the range from 145°C to 175°C, while the PET core and PET2 skin components have T_m above 230°C. PET1 skin is an amorphous polymer; therefore, it does not melt but only softens at elevated temperatures (T_g above 75°C). Considering the standard lamination conditions developed for the production of glass-based PV modules with EVA encapsulants and polymeric backsheets, the melting temperatures of PP are relatively low. Hence, PP HSC would require an adaptation of the lamination temperature and the careful selection of encapsulants that can be processed at temperatures below 140°C, such as TPOs. However, PET HSC have none or high melting temperatures and should be compatible with commonly used encapsulants, like EVA and crosslinking polyolefins (POEs) or combinations thereof (EPE).

Results of the heat conductivity (λ) measurements show that HSCs are insulating materials, with values below 0.2 $W m^{-1} K^{-1}$ for all material combinations investigated, as shown in Figure 6.

Furthermore, HSCs exhibit λ values up to five times lower than glass ($\lambda = 1 W m^{-1} K^{-1}$) [44]. As c-Si solar cells convert only a portion (~20%–23%) of the absorbed light into electricity and the rest into heat, thermally conductive materials surrounding solar cells are preferred to enhance heat dissipation. Low heat conductivity of insulating materials leads to increased operational temperatures of the PV module, negatively impacting the efficiency of solar cells, as well as the reliability and durability of both the module and its components, especially polymers [4, 45]. Research by Özkalay et al. [46] determined the maximum operating temperatures (T_{max}) for identical modules in open-rack and BIPV systems and evaluated their impact on module efficiency and long-term performance. T_{max} measured for open-rack PV modules in both glass/glass and glass/backsheet configurations was approximately 60°C during the operational hours. In contrast, ventilated and insulated BIPV modules exhibited higher T_{max}, slightly above 80°C and 90°C, respectively [46].

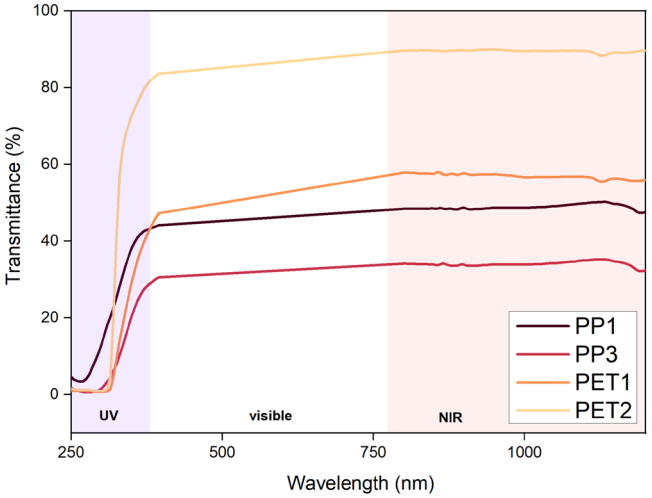

FIGURE 4 | UV—vis—NIR spectra of honeycomb skins. [Color figure can be viewed at wileyonlinelibrary.com]

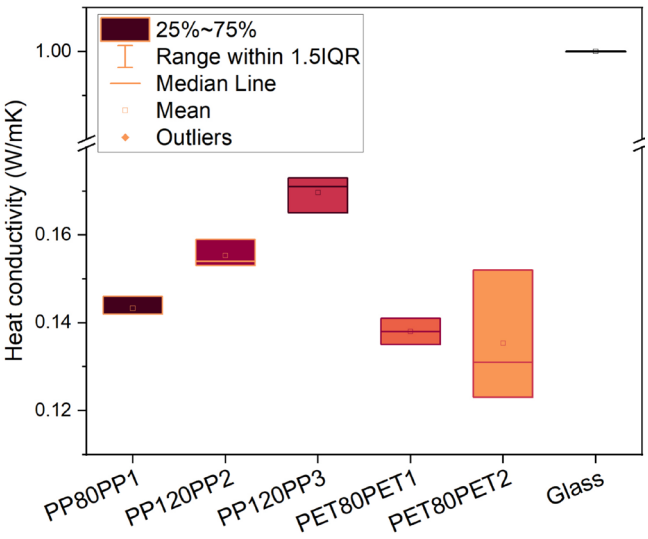

FIGURE 6 | Heat conductivity of the honeycomb sandwich composites and glass. [Color figure can be viewed at wileyonlinelibrary.com]

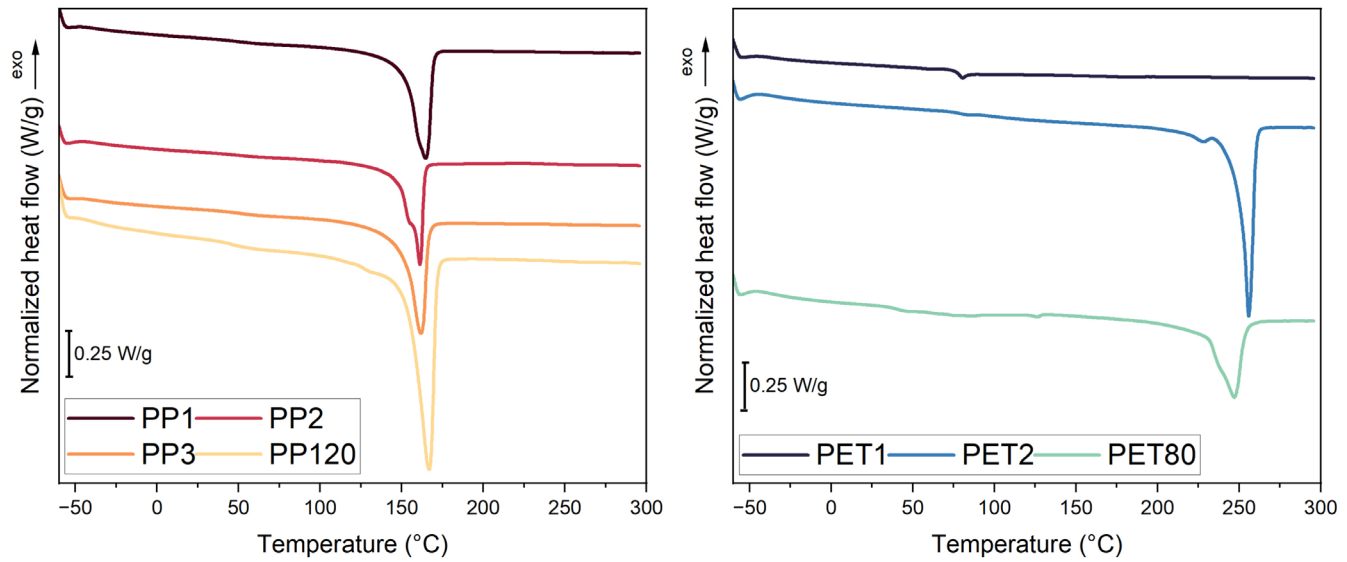

FIGURE 5 | DSC first heating curves of honeycomb components. [Color figure can be viewed at wileyonlinelibrary.com]

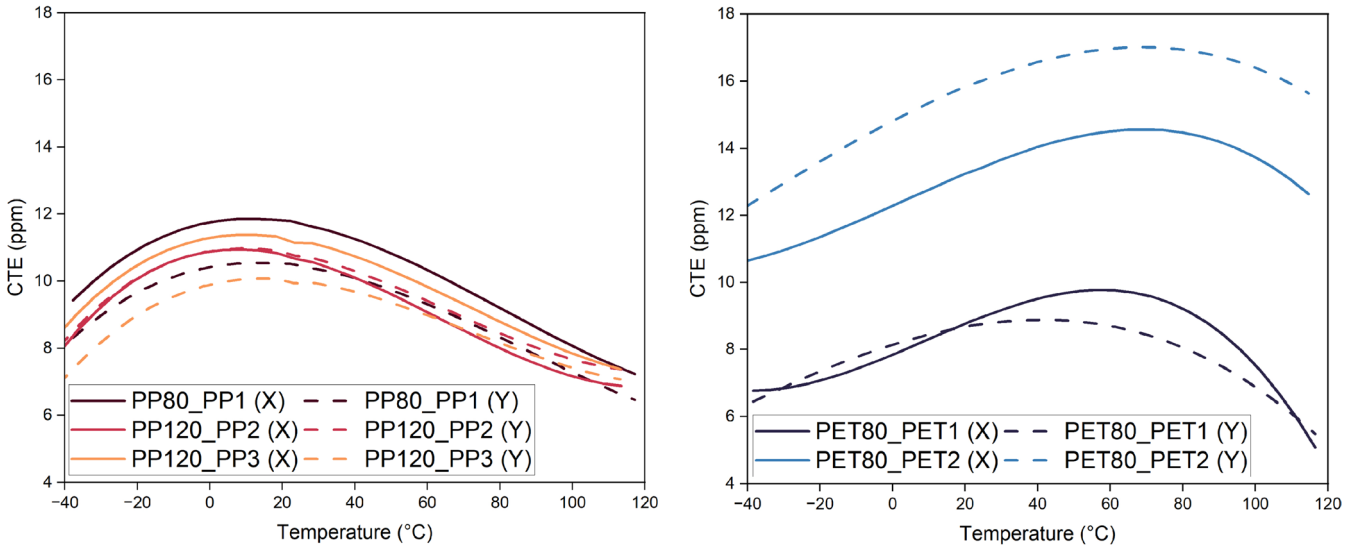

FIGURE 7 | CTE graphs of honeycomb skins (left side PP- and right side PET-based HSC). [Color figure can be viewed at wileyonlinelibrary.com]

Based on these data, similar behavior could be expected when HSCs are integrated as the backsides in lightweight PV modules. Additionally, a challenge can arise during the lamination process as heat conduction and distribution within the PV module can take longer, unless the lamination process is performed by placing the front side of the module on the hot plate. On the positive side, this reduced heat conductivity could provide a benefit in terms of thermal insulation for the building interior to which these PV modules are attached, such as façades or roofing elements [47].

In addition to differences in T_{max} of the modules installed in the open-rack and BIPV configuration, significant day–night temperature variations exceeding 75°C for insulated BIPV modules were measured [46]. These daily temperature fluctuations impact the thermomechanical material behavior of the materials within the module stack, and an inherent mismatch in the CTE between the individual material layers can create internal stresses resulting in interlayer delamination, failures of solder joints, and solar cell cracking [4, 48]. Therefore, careful consideration of the bill of materials (BoM) is essential when selecting components for lightweight PV modules.

The dimensional stability and mechanical behavior of the HSC materials at different temperatures, in terms of CTE, are presented in Figure 7. The HSC skins PP1, PP2, PP3, and PET1 with GFR exhibit comparable behavior in the *x*- and *y*-directions due to the presence of the GFs in 0°–90° ply orientation. These materials show numerical CTE values between 6 and 12 ppm within the temperature range from −40°C to 120°C. The PET2 skin, a biaxially oriented PET material, shows slightly higher CTE values, 10–17 ppm, in the same temperature range, but with a somewhat greater anisotropy in the *x*- and *y*-directions compared to the GFR skins. All HSC skins investigated exhibit low anisotropy and lower CTE values than those of commonly used commercial polymer backsheets (e.g., TPT, coated PET [CPC], coextruded PP, triple polyamide [AAA]) [49, 50]. Additionally, CTE values of GFR HSCs can be compared to those of glass reported in the literature [51] and measured in-house (see Table 2). Given this similar thermomechanical behavior, GFR HSCs are expected to exhibit comparable performance to glass when integrated as a backsheet in a PV module.

3.3 | Mechanical Properties

Upon visual observation, HSC are a thicker product (10.3–12 mm, see Table 1), particularly when compared to standard polymeric backsheets (0.5 mm) or glass backsheets (3.2 mm). On the other hand, the honeycomb-metamaterial core significantly reduces the weight of the composite while enhancing its mechanical strength. When HSC (areal density = 1.82 kg m^{-2}) are implemented as backsheets, the need for a solar glass frontsheet (areal density = 8 kg m^{-2} [52]) can be eliminated, resulting in a reduction of the PV module's weight by up to a factor of four [26].

Load vs. displacement diagrams of the four-point bending tests are shown in Figure 8. The PP80_PP1 HSC was excluded from the test due to the high WVTR and thin wall of the core's cell. The PET-based HSC failed under the compression stress upon reaching its maximum load carrying capacity. On the other hand, the PP-based HSC yielded above the maximum carrying load. This behavior could be due to the fact that at room temperature PET remains in a glassy state (T_g = 80°C, Figure 5), which can restrict the mobility of the chains; hence, resulting in a brittle-like failure. When comparing the mechanical behavior of the PP-based HSC, PP120_PP3 shows greater stiffness (as indicated by the steeper slope in the load-line displacement diagram in the elastic region) and greater load carrying capacity compared to PP120_PP2. This could be connected with the better embedment of the GF in the polymer matrix in PP3 skin when compared to PP2 (see Figure 2).

3.4 | Accelerated Aging Influence on Properties

The longevity of the electricity generation of PV modules is directly linked to the performance of the envelope materials. To ensure a long lifetime, reliability, and maintained efficiency of PV modules, the durability of the materials used in the PV modules needs to be characterized. Material behavior/degradation is best understood

through outdoor testing; this is time-consuming, in particular considering targeted lifetimes of 25 years and beyond. Therefore, indoor artificial aging tests and material characterization methods are typically used to determine reliability and material properties post aging. In this study, a DH test was performed according to IEC 61215, and DSC and TGA characterization methods were done to characterize material state and changes that occurred during the exposure period. Additionally, to investigate water condensation within the hollow cell space of the core layer, HSC were placed in the climate chamber under continuous heating and cooling cycles (from 85°C to 5°C, with 85% humidity) for 30 days.

Upon the accelerated aging, yellowing of the PP HSC was observed, similar to the observation by other studies [5]. Thermal aging affects the stability of additives in the PP matrix, which then change color; however, the effect is reversible after photobleaching [53]. The cooling thermograms from DSC for PP core and PP3 skin material in Figure 9 show no significant changes in the crystallization temperature (T_c), meaning that DH aging left no apparent impact on the polymer matrix. This was similarly observed for commercially available PP backsheets [28, 53–54]. However, a shift to higher T_c values was observed for the PP2 skin, rPET core, and PET2 skin, from 118°C to 124°C, 206°C to 218°C, and 176°C to 186°C, respectively. This shift, indicating an earlier onset of crystallization, occurs due to the chain scission in both PP and PET polymer [55, 56]. This phenomenon has already been reported by Oreski et al., where the authors determined that critical crystallization temperatures between 208°C and 211°C correspond to a reduction in molar mass and severe embrittlement of PET [56]. Lamentably, DH aging resulted in a shift of T_c above the critical values for rPET, and consequently in the loss of mechanical properties, making the rPET core prone to cracking and structural failure under an external mechanical load. Anti-hydrolysis additives can be added to the PET polymer matrix to mitigate the chain-scission process and ensure mechanical strength [57].

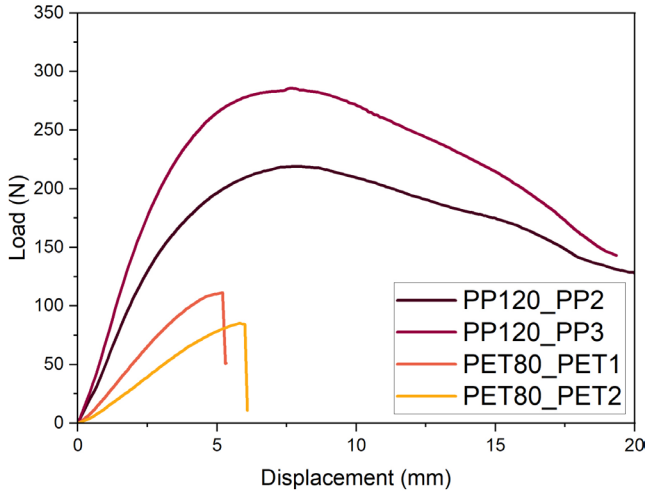

FIGURE 8 | Load versus displacement diagram of PP and PET based HSC under flexural loading. [Color figure can be viewed at wileyonlinelibrary.com]

Aging under the DH conditions also resulted in the earlier material decomposition of both PP and rPET core materials, evident for both materials in Figure 10. The change in the onset decomposition temperature marked by the temperature at which 5% of weight loss ($T_{5\%}$) occurs is more pronounced for the rPET core, where the $T_{5\%}$ shifted from 394°C before aging to 385°C after aging. In contrast, for the PP material, $T_{5\%}$ shifted from 430°C to 428°C after aging. Of all skin materials, only PP2 skin showed earlier decomposition onset, which shifted by 5°C compared to the unaged sample. The polymer chain scission created smaller molecules that are decomposing into volatile products faster; therefore, $T_{5\%}$ shifted toward the lower temperatures.

The water condensation test resulted in a weight gain of less than 0.2 wt% for all HSC samples. Since no established standard could be found for it, an in-house created test procedure was followed. The relatively low weight gain of these materials may be attributed to the "breathability" of the composite's outer skins, which allow moisture vapor transmission and thus prevent water condensation within the closed hexagonal cells of the core. Alternatively, it

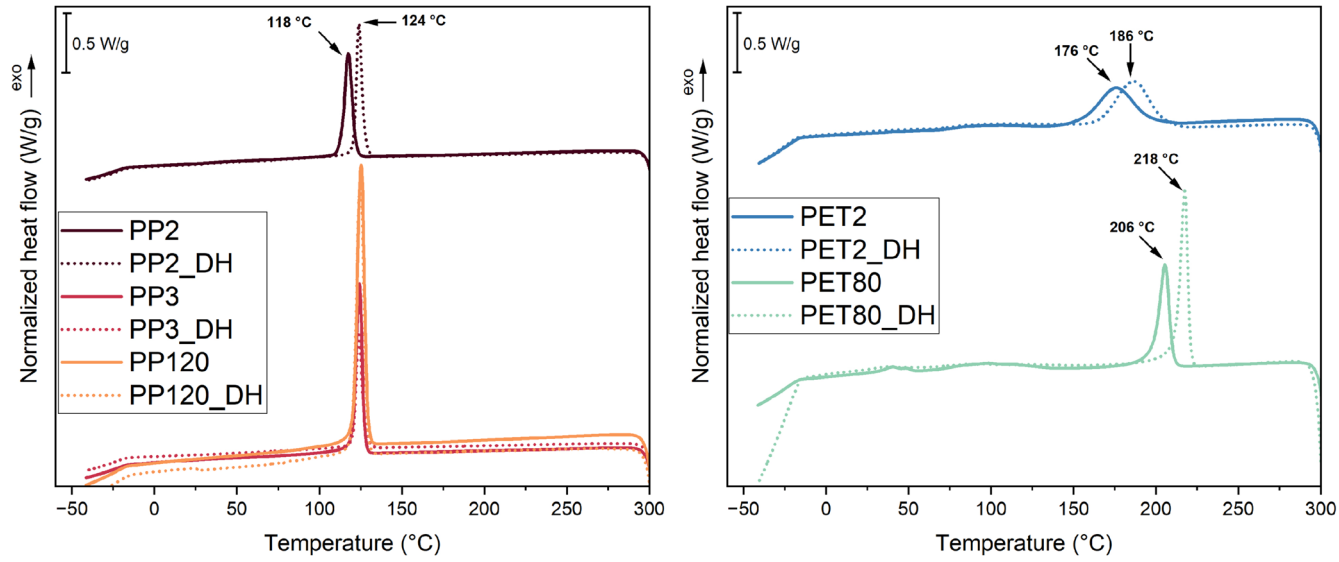

FIGURE 9 | DSC cooling curves of unaged and aged PP and PET. [Color figure can be viewed at wileyonlinelibrary.com]

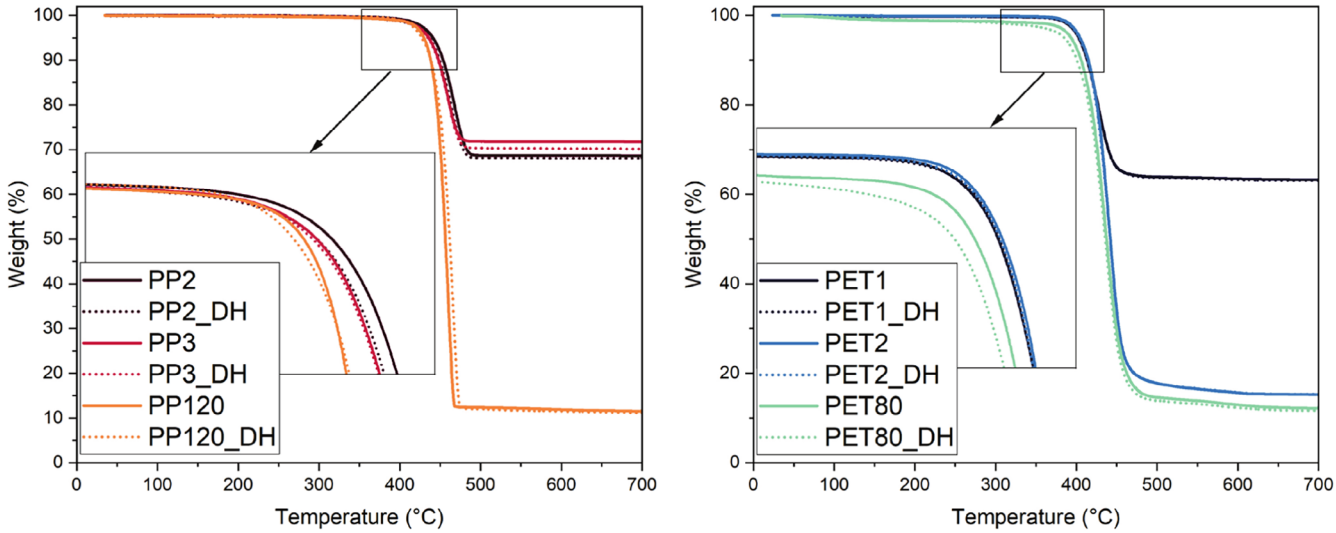

FIGURE 10 | TGA curves of core material before and after aging. [Color figure can be viewed at wileyonlinelibrary.com]

is possible that the test procedure itself needs further adaptation to create better conditions for water condensation. Nevertheless, it can be concluded that no significant weight gain is expected for BAPV and BIPV modules with HSC backsheets under the heating and cooling conditions typically encountered during outdoor exposure. This property brings a positive impact, as water will not accumulate in the hollow areas and impact overall weight, material durability, and mold growth [4].

4 | Conclusions

The selected, commercially available PP and PET HSC, already used in building and automotive industries, proved to be promising materials for the backside integration into the lightweight PV modules. Results have shown that proper GF embedment within the polymer matrix, in the GFRP skin material, improves the mechanical properties of entire sandwich composites and reduces WVTRs. Semitransparent skins with transmission in the NIR and visible light spectra could enable bifacial PV modules but require the addition of the UV absorbers to ensure long-term stability of HSC components and of the internal module components (encapsulants and solar cells). HSCs exhibit glass-like thermomechanical behavior but low thermal conductivity, which could affect module temperature regulation and negatively impact efficiency. DH exposure caused minor degradation in PP-based materials, which resulted in yellowing, while PET materials experienced more prominent polymer chain scission and significant material embrittlement, which indicates the need for improved hydrolysis resistance. Further investigation is required to assess mechanical reliability. Replacing the glass front-sheet and removing the aluminum frame are considered feasible, though evaluation is still ongoing.

Author Contributions

Nikolina Pervan: conceptualization (equal), data curation (lead), formal analysis (lead), investigation (lead), methodology (equal), visualization (lead), writing – original draft (lead). **Umang Desai:** conceptualization (equal), data curation (supporting), formal analysis (supporting), investigation (supporting), methodology (supporting), visualization (supporting), writing – original draft (supporting). **Gabriele C. Eder:** conceptualization (equal), writing – review and editing (equal). **Jonathan Govaerts:** conceptualization (equal), writing – review and editing (equal). **Arne Derluyn:** resources (equal). **Wouter Winant:** resources (equal), writing – review and editing (equal). **Antonin Faes:** writing – review and editing (supporting). **Christophe Ballif:** writing – review and editing (supporting). **Gernot Oreski:** conceptualization (equal), funding acquisition (lead), project administration (lead), resources (equal), supervision (lead), writing – review and editing (lead).

Acknowledgments

The research work of this paper was performed at the Polymer Competence Center Leoben GmbH (PCCL, Austria) as part of the Solar Era Net Project "DELIGHT," which is supported under the umbrella of SOLAR-ERA.NET co-fund by the Austrian Research Promotion Agency (FFG, contract number FO999897443) and the Swiss Federal Office of Energy (SFOE, contract number SI/502501-01). SOLAR-ERA.NET is supported by the European Commission within the EU Framework Programme for Research and Innovation HORIZON 2020 (co-fund ERA-NET Action, No. 691664). N/A

Conflicts of Interest

The authors declare no conflicts of interest.

Data Availability Statement

The data that support the findings of this study are available on request from the corresponding author. The data are not publicly available due to privacy or ethical restrictions.

References

1. The European Parliament and the Council of the European Union, "Directive (EU) 2023/2413 of the European Parliament and of the Council of 18 October 2023 Amending Directive (EU) 2018/2001, Regulation (EU) 2018/1999 and Directive 98/70/EC as Regards THE Promotion of Energy From Renewable Sources, and Repealing Council Directive (EU) 2015/652," *Official Journal of the European Union* L series (2023).

2. J. K. Nøland, J. Auxepaules, A. Rousset, B. Perney, and G. Falleti, "Spatial Energy Density of Large-Scale Electricity Generation From Power Sources Worldwide," *Scientific Reports* 12 (2022): 21280.

3. M. Deshaies, "Problèmes géographiques des transitions énergétiques quelles perspectives pour l'évolution du système énergétique ?," *Mondes En Développement* 192 (2020): 25–44.

4. N. M. Chivelet, C. Kapsis, and F. Frontini, *Building-Integrated Photovoltaics: A Technical Guidebook*, 1st ed. (Routledge, 2024).

5. G. Oreski, J. S. Stein, G. C. Eder, et al., "Motivation, Benefits, and Challenges for New Photovoltaic Material & Module Developments," *Progress in Energy* 4 (2022): 32003, https://doi.org/10.1088/2516-1083/ac6f3f.

6. IEA PVPS, "Fire Safety of BIPV: International Mapping of Accredited and R&D Facilities in the Context of Codes and Standards 2023," Report (IEA PVPS, 2023).

7. National Heritage Institute, *Photovoltaic Systems in Heritage Protection* (National Heritage Institute, 2022).

8. G. Eder, G. Peharz, R. Trattnig, et al., "COLOURED BIPV—Market, Research and Development," 2019 Report IEA-PVPS T15-07: 2019 (IEA-PVPS, 2019).

9. N. Pervan, S. Feldbacher, M. Harnisch, T. Tettenborn, A. Zimmermann, and G. Oreski, eds., *Ultra-Thin Flexible Glass as Environmental Shield for CIGS Photovoltaic Modules*, EU PVSEC 2024, ISBN 3-936338-90-6, 2024.

10. IEA PVPS, *Successful Building Integration of Photovoltaics—A Collection of International Projects* (IEA PVPS, 2021).

11. A. C. Martins, V. Chapuis, F. Sculati-Meillaud, A. Virtuani, and C. Ballif, "Light and Durable: Composite Structures for Building-Integrated Photovoltaic Modules," *Progress in Photovoltaics: Research and Applications* 26 (2018): 718–729, https://doi.org/10.1002/pip.3009.

12. A. C. Oliveira Martins, V. Chapuis, A. Virtuani, L.-E. Perret-Aebi, and C. Ballif, "Hail Resistance of Composite-Based Glass-Free Lightweight Modules for Building Integrated Photovoltaics Applications," in *Proceedings of the 33rd European Photovoltaic Solar Energy Conference and Exhibition* (EPFL, 2017), 2604–2608.

13. A. C. Martins, V. Chapuis, A. Virtuani, and C. Ballif, "Robust Glass-Free Lightweight Photovoltaic Modules With Improved Resistance to Mechanical Loads and Impact," *IEEE Journal of Photovoltaics* 9 (2019): 245–251, https://doi.org/10.1109/JPHOTOV.2018.2876934.

14. A. C. Martins, V. Chapuis, A. Virtuani, H.-Y. Li, L.-E. Perret-Aebi, and C. Ballif, "Thermo-Mechanical Stability of Lightweight Glass-Free Photovoltaic Modules Based on a Composite Substrate," *Solar Energy Materials & Solar Cells* 187 (2018): 82–90, https://doi.org/10.1016/j.solmat.2018.07.015.

15. P. Grygiel, J. Tarłowski, M. Prześniak-Welenc, et al., "Prototype Design and Development of Low-Load-Roof Photovoltaic Modules for Applications in On-Grid Systems: Solar Energy Materials and Solar Cells," *Solar Energy Materials and Solar Cells* 233 (2021): 111384.

16. C. Kutter, F. Basler, L. E. Alanis, J. Markert, M. Heinrich, and D. H. Neuhaus, eds., "Integrated Lightweight, Glass-Free PV Module Technology for Box Bodies of Commercial Trucks," in *37th European Photovoltaic Solar Energy Conference and Exhibition, EU PVSEC 2020* (Fraunhofer-Gesellschaft, 2020), 1711–1718.

17. L. E. Alanis, A. Velte-Schäfer, N. Jajoo, et al., "Thermal Effect of VIPV Modules in Refrigerated Trucks," *Solar Energy Materials and Solar Cells* 275 (2024): 113000.

18. A. Omazic, G. Oreski, M. Halwachs, et al., "Relation Between Degradation of Polymeric Components in Crystalline Silicon PV Module and Climatic Conditions: A Literature Review," *Solar Energy Materials & Solar Cells* 192 (2019): 123–133, https://doi.org/10.1016/j.solmat.2018.12.027.

19. G. Oreski, C. Barretta, L. Castillon, P. Christöfl, and M. Köntges, "Importance of Bill of Material (BOM) Control and IEC 61215 Scope of Application," in *37th European Photovoltaic Solar Energy Conference and Exhibition* (EU PVSEC, 2020).

20. G. Oreski, A. Mihaljevic, Y. Voronko, and G. C. Eder, "Acetic Acid Permeation Through Photovoltaic Backsheets: Influence of the Composition on the Permeation Rate," *Polymer Testing* 60 (2017): 374–380, https://doi.org/10.1016/j.polymertesting.2017.04.025.

21. DuPont Photovoltaic Solutions, *DuPont Global PV Reliability: 2020 Field Analysis* (DuPont Photovoltaic Solutions, 2020).

22. S. Uličná, R. L. Arnold, J. M. Newkirk, et al., "Material Characterization of Seven Photovoltaic Backsheets Using Seven Accelerated Test Conditions," *Solar Energy Materials and Solar Cells* 267 (2024): 112726.

23. J. Govaerts, P. Dufke, B. Luo, et al., eds., "Light as Heaven, Strong as Hell(?): Testing Honeycomb-Based Laminates for Light-Weight c-Si PV Applications," in *Proceedings of the 40th European Photovoltaic Solar Energy Conference and Exhibition* (EU PVSEC, 2023).

24. IEC, "IEC 61215-1:2021, Terrestrial Photovoltaic (PV) Modules—Design Qualification and Type Approval—Part 1: Test Requirements," 2021.

25. ASTM International, "Standard Test Method for Evaluating the Resistance to Thermal Transmission of Materials by Guarded Heat Flow Meter Technique," 2019.

26. U. Desai, M. Courtant, G. Eder, G. Oreski, A. Faes, and C. Ballif, "Novel Mechanically Robust and Environmentally Stable Light-Weight Colored Photovoltaic Modules Based on Composite Polymer Backsheets," *Solar RRL* 9 (2025): 2500177.

27. DuPont, "DuPont Tedlar Polyvinyl Fluoride (PVF) Films," 2014, https://www.dupont.com/content/dam/dupont/amer/us/en/photovoltaic/public/documents/DEC_Tedlar_GeneralProperties1.pdf.

28. A. Omazic, G. Oreski, M. Edler, et al., "Increased Reliability of Modified Polyolefin Backsheet Over Commonly Used Polyester Backsheets for Crystalline PV Modules," *Journal of Applied Polymer Science* 137 (2020): 48899, https://doi.org/10.1002/app.48899.

29. M. Babin, G. C. Eder, Y. Voronko, and G. Oreski, "Water Vapor Permeability of Polymeric Packaging Materials for Novel Glass-Free Photovoltaic Applications," *Journal of Applied Polymer Science* 141 (2024): e55733, https://doi.org/10.1002/app.55733.

30. Fraunhofer UMSICHT, "End-of-Life Pathways for Photovoltaic Backsheets: End-of-Life Treatment—Experiments, Germany," Report (Fraunhofer UMSICHT, 2017).

31. M. Knausz, G. Oreski, G. C. Eder, et al., "Degradation of Photovoltaic Backsheets: Comparison of the Aging Induced Changes on Module and Component Level," *Journal of Applied Polymer Science* 132 (2015): 1–8, https://doi.org/10.1002/app.42093.

32. J. Zhou, Z. Zhang, H. Liu, and Q. Yi, "Temperature Distribution and Back Sheet Role of Polycrystalline Silicon Photovoltaic Modules," *Applied Thermal Engineering* 111 (2017): 1296–1303.

33. B. Luo, J. Govaerts, F. Lisco, et al., "Encapsulation Strategies for Mechanical Impact and Damp Heat Reliability Improvement of Lightweight Photovoltaic Modules Towards Vehicle-Integrated Applications," *Solar Energy Materials and Solar Cells* 273 (2024): 112932.

34. C. Tselios, D. Bikiaris, P. Savidis, C. Panayiotou, and A. Larena, "Glass-Fiber Reinforcement of In Situ Compatibilized Polypropylene/Polyethylene Blends," *Journal of Materials Science* 34 (1999): 385–394.

35. A. Baker, S. Dutton, and D. Kelly, *Composite Materials for Aircraft Structures* (American Institute of Aeronautics and Astronautics, 2004).

36. Y. Fu and X. Yao, "A Review on Manufacturing Defects and Their Detection of Fiber Reinforced Resin Matrix Composites," *Composites Part C: Open Access* 8 (2022): 100276.

37. O. K. Segbefia, A. G. Imenes, and T. O. Sætre, "Moisture Ingress in Photovoltaic Modules: A Review," *Solar Energy* 224 (2021): 889–906.

38. H. E. Yang, R. H. French, and L. S. Bruckman, eds., *Durability and Reliability of Polymers and Other Materials in Photovoltaic Modules* (William Andrew Publishing, 2019).

39. Y. Voronko, G. C. Eder, M. Knausz, G. Oreski, T. Koch, and K. A. Berger, "Correlation of the Loss in Photovoltaic Module Performance With the Ageing Behaviour of the Backsheets Used," *Progress in Photovoltaics Research and Applications* 23 (2015): 1501–1515, https://doi.org/10.1002/pip.2580.

40. S. Uličná, A. Sinha, D. C. Miller, B. M. Habersberger, L. T. Schelhas, and M. Owen-Bellini, "PV Encapsulant Formulations and Stress Test Conditions Influence Dominant Degradation Mechanisms," *Solar Energy Materials & Solar Cells* 255 (2023): 112319, https://doi.org/10.1016/j.solmat.2023.112319.

41. J. Smoleń, K. Bechcińska, W. Smok, P. Olesik, and K. Stępień, "Assessment of the Effectiveness of Selected Coatings for Protection Against UV Radiation in Glass Fiber Reinforced Composites (GFRP)," *Composites Theory and Practice* 24 (2024): 65–71.

42. G. Demircan, M. Kisa, M. Ozen, A. Acikgoz, Y. Işıker, and E. Aytar, "Nano-Gelcoat Application of Glass Fiber Reinforced Polymer Composites for Marine Application: Structural, Mechanical, and Thermal Analysis," *Marine Pollution Bulletin* 194 (2023): 115412.

43. R. E. Fyfe, "Fire Protection Coating for FRP-Reinforced Structure", Patent "US20090075051A1," 2009.

44. Schott AG, "TIE-31: Mechanical and Thermal Properties of Optical Glass," 2004, https://www.schott.com/shop/medias/schott-tie-31-mechanical-and-thermal-properties-of-optical-eng.pdf?context=bWFzdGVyfHJvb3R8MjIxODU3fGFwcGxpY2F0aW9uL3BkZnxoYjkvaGI0Lzg4MjAyMzc5MjY0MzAucGRmfGJmMzI4ZjE5ZTEyNzdiMjRkYWQ5Y2QyOWFiNmU1MTU5ZDdmMWJjZDFlODEwZTllMjlkMjk1ZWEzN2JlNjY5MjI.

45. E. Özkalay, A. Virtuani, G. Eder, et al., "Correlating Long-Term Performance and Aging Behaviour of Building Integrated PV Modules," *Energy and Buildings* 316 (2024): 114252, https://doi.org/10.1016/j.enbuild.2024.114252.

46. E. Özkalay, G. Friesen, M. Caccivio, et al., "Operating Temperatures and Diurnal Temperature Operating Temperatures and Diurnal Temperature Variations of Modules Installed in Open-Rack and Typical BIPV Configurations," *IEEE Journal of Photovoltacis* 12 pages: 133–140, 2022.

47. H. P. Ebert, "Functional Materials for Energy-Efficient Buildings," *EPJ Web of Conferences* 68 (2015): 08001.

48. G. C. Eder, Y. Voronko, G. Oreski, et al., "Error Analysis of Aged Modules With Cracked Polyamide Backsheets," *Solar Energy Materials and Solar Cells* 203 (2019): 110194.

49. P. Romer, G. Oreski, A. J. Beinert, H. Neuhaus, and M. Mittag, "More Realistic Considerations of Backsheets Coefficient of Thermal Expansion on Thermomechanics of PV Modules," in *37th European Photovoltaic Solar Energy Conference and Exhibition* (EUPVSEC, 2020), 772–776.

50. P. Fuchs, A. Halm, and M. Klenk, eds., "FEM Simulation of Influence of Different Polymeric Module Materials and Layouts on Thermomechanical Deformations in Strings of Shingled Solar Cells," in *2023 24th International Conference on Thermal, Mechanical and Multi-Physics Simulation and Experiments in Microelectronics and Microsystems (EuroSimE)* (IEEE, 2023).

51. M. Knausz, G. Oreski, M. Schmidt, et al., "Thermal Expansion Behavior of Solar Cell Encapsulation Materials," *Polymer Testing* 44 (2015): 160–167, https://doi.org/10.1016/j.polymertesting.2015.04.009.

52. Glass Technology Services, "Glass Weight Calculator," accessed March 28, 2025, https://www.glass-ts.com/resources/glass-weight-calculator/results.

53. G. Oreski, C. Barretta, A. Macher, et al., "Investigation of the Crack Propensity of Co-Extruded Polypropylene Backsheet Films for Photovoltaic Modules," *Solar Energy Materials and Solar Cells* 259 (2023): 112438.

54. A. Aiello, S. Mitterhofer, J. Obrzut, et al., "A Spatially Resolved Evaluation of Accelerated Environmental Aging on Emerging Polypropylene-Based Photovoltaic Backsheets Using Raman Spectroscopy," *Progress in Photovoltaics: Research and Applications* 33 (2025): 652–662.

55. W. Camacho and S. Karlsson, "Assessment of Thermal and Thermo-Oxidative Stability of Multiextruded Recycled PP, HDPE and a Blend Thereof," *Polymer Degradation and Stability* 78 (2002): 385–391.

56. G. Oreski, B. Ottersböck, C. Barretta, P. Christöfl, S. Radl, and G. Pinter, "Degradation of PET—Quantitative Estimation of Changes in Molar Mass Using Mechanical and Thermal Characterization Methods," *Polymer Testing* 125 (2023): 108130.

57. B. Ottersböck, G. Oreski, and G. Pinter, "Correlation Study of Damp Heat and Pressure Cooker Testing on Backsheets," *Journal of Applied Polymer Science* 133 (2016): 44230, https://doi.org/10.1002/app.44230.